Persistent currents in toroidal carbon nanotubes

M. F. Lin
Department of Physics, National Cheng Kung University, Tainan 70101, Taiwan, Republic of China

D. S. Chuu
Electrophysics Department, National Chiao Tung University, Hsinchu 30050, Taiwan, Republic of China

(Received 27 May 1997)

The geometric structure of the toroidal carbon nanotubes (TCN's) determines the electronic structure and thus the characteristics of the persistent current. Such current is caused by the magnetic flux ϕ through TCN's. The semiconducting TCN's exhibit diamagnetism at small ϕ, which is in great contrast with paramagnetism of the metallic TCN's. The induced magnetic moment is proportional to the toroid radius, but independent of the toroid width. The magnetic response is weak, while it is much stronger than that of a mesoscopic semiconductor or metal ring. The persistent current is a linearly periodical function of ϕ, with a period $\phi_0(hc/e)$. Such an oscillation is the manifestation of the Aharonov-Bohm (AB) effect. Temperature (T) does not destroy the periodical AB oscillation, although it would significantly reduce the persistent currents. The Zeeman splitting may lead to the destruction of the periodicity at very large ϕ. A larger TCN at lower T and ϕ is relatively suitable for verifying the AB effect. [S0163-1829(98)01412-X]

I. INTRODUCTION

Carbon nanotubes have attracted a lot of attention since their discovery in 1991 by Iijima.[1] Each straight carbon nanotube (SCN) could be regarded as a rolled-up graphite sheet in cylindrical form. Its radius (r) is only between 10 and 150 Å, while its length is more than 1 μm. Carbon nanotubes could bend within the crystalline rope;[2] moreover, the two ends are found to be able to be knit together seamlessly.[3] Carbon atoms could form a toroidal carbon nanotube [(TCN) or a carbon toroid], with an average radius $R\sim 1500-2500$ Å. The toroid radius is much larger than the height or the width ($\sim$10 Å). A very thin TCN is basically similar to a mesoscopic metal[4–6] or semiconductor[7] ring. TCN's, as with mesoscopic rings, would be the ideal system for verifying certain quantum effects, e.g., the persistent currents (I's).[4–7] Such currents are purely due to magnetic flux (ϕ) through TCN's. The electronic structure of the TCN's and the characteristics of the persistent currents are studied in this work. The dependence of the persistent current on the magnetic flux, the electronic structure, the toroid radius (R), the temperature (T), and the Zeeman splitting is investigated. A comparison between TCN's and SCN's Refs. 8–10 will be made.

The toroidal forms of graphitic carbons could be constructed from nanotubes by (1) connecting small sliced parts of the nanotubes,[11] (2) connecting two sections of identical turnover bilayer nanotube ends at the equator of the resulting toroid,[12] and (3) bending a long nanotube and connecting its ends together (this work). Dunlap first proposed the carbon toroids C_{576} and C_{540} by connecting the sliced parts of nanotubes.[11] Later the second kind of carbon toroids were proposed by Itoh *et al.*[12] These two kinds of carbon toroids have certain pentagons and heptagons instead of hexagons, while the third kind of carbon toroid is purely made from the distorted hexagonal lattices. The former have the ratio $R/r<10$, which is much smaller than that (>100) of the latter. Hence the geometric structures of the first and the second kinds of carbon toroids are quite different than those studied in this work.

The tight-binding model[13] has been used to study the π-electronic structure of a SCN.[14] It is similar to that employed for a graphite sheet, but with the periodical boundary condition along the transverse direction. The electronic states of a TCN are further obtained, when the periodical boundary condition along the axial direction is also applied. A TCN owns many discrete states, mainly owing to the transverse and longitudinal boundary conditions. It may be a metal or a semiconductor, which is closely related to the geometric structure. A semiconducting TCN has an energy gap (E_g) between the highest occupied states (HOS) and the lowest unoccupied states (LUS). But for a metallic TCN, both HOS and LUS are just located at the Fermi level ($E_F=0$).[15,16] The characteristics of the electronic structures will be directly reflected in the persistent current. A TCN would drastically change from a metal (semiconductor) to a semiconductor (metal) during the variation of ϕ. As a result of the large R, the Zeeman effect is generally negligible except at very large ϕ. The ϕ-dependent electronic states are periodical in ϕ, with a period $\phi_0=hc/e$, as are the persistent currents. This is the so-called Aharonov-Bohm (AB) effect. In general, such an effect is present in toroidal[3,17] and cylindrical[1] systems.

Haddon[17] had studied the magnetic properties of the C_{576} toroid.[11] It is predicted to exhibit diamagnetism. The magnetism of the thin TCN's will be investigated. There are certain theoretical predictions concerning the magnetic response of SCN's.[8–10] The induced magnetic moment is independent of radius. Metallic and semiconducting SCN's at $\phi=0$, respectively, exhibit the paramagnetic and diamagnetic behavior at small ϕ. The magnetic response is predicted to be observable at $T<100$ K. Moreover, the Zeeman splitting could cause the special cusp structures and destroy the periodicity of the

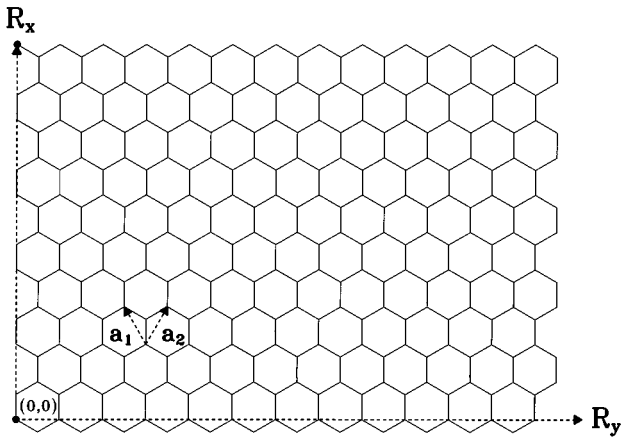

FIG. 1. A toroidal carbon nanotube could be regarded as a finite graphite sheet rolled from the origin to the vectors $\mathbf{R}_x = m\mathbf{a}_1 + n\mathbf{a}_2$ and $\mathbf{R}_y = p\mathbf{a}_1 + q\mathbf{a}_2$ simultaneously. $\mathbf{a}_1$ and $\mathbf{a}_2$ are the primitive vectors of the graphite sheet.

AB oscillation.[10] We will study whether TCN's exhibit similar properties.

Three successful experimental investigations demonstrate that persistent currents exist in mesoscopic metal[5–6] and semiconductor[7] rings. The magnetic moment induced by the persistent current is $\sim 10^{-20}$–10^{-22} Å m^2, and its magnitude rapidly decreases in the increasing of T. The magnetic moment in a mesoscopic ring is found to be much smaller than that in a thin TCN. Hence the persistent currents in TCN's are observable in the low-temperature magnetic measurements.

This paper is organized as follows. In Sec. II, the π-electronic structure of a thin TCN threaded by a uniform perpendicular magnetic field (B) is calculated from the tight-binding model. The persistent currents are evaluated in Sec. III. The main features are discussed, and certain effects are investigated. Concluding remarks are made in Sec. IV.

II. ELECTRONIC STATES IN A B FIELD

We first see the geometric structure of a SCN. It is formed by rolling a graphite sheet from the origin to the vector $\mathbf{R}_x = m\mathbf{a}_1 + n\mathbf{a}_2$, where $\mathbf{a}_1$ and $\mathbf{a}_2$ are the primitive lattice vectors of the graphite sheet (Fig. 1). A SCN is equivalent to a graphite sheet which satisfies the periodical boundary condition along the transverse direction. The parameters (m,n) are used to characterize a SCN. There are two kinds of achiral SCN's. One is the (m,m) armchair nanotube,[18] and the other is the $(m,0)$ zigzag nanotube. They, respectively, have zigzag and armchair structures along the longitudinal direction (parallel to $\mathbf{R}_y = p\mathbf{a}_1 + q\mathbf{a}_2$). The armchair nanotubes are found to be the principal constituents of the crystalline rope.[2] Furthermore, they might be the precursors of the TCN's.[3]

A carbon nanotube could bend so that the two ends are able to knit together. A TCN corresponds to a finite graphite sheet which is rolled from the origin to the vectors $\mathbf{R}_x$ and $\mathbf{R}_y$ simultaneously. That is to say, a TCN satisfies the periodical boundary conditions along the transverse and longitudinal directions. The parameters (m,n,p,q), therefore, uniquely define a TCN.[19] Here we mainly focus on the TCN's, which have armchair structure along the transverse direction and zigzag structure along the longitudinal direction, and vice versa. They are called armchair $(m,m,-p,p)$ and zigzag $(m,0,-p,2p)$ TCN's, respectively. Other TCN's derived from the chiral nanotubes are expected to exhibit similar electronic properties.

The π-electronic structure of a TCN, as done in a graphite sheet,[13] is calculated by the tight-binding model. A TCN here is in the presence of a uniform perpendicular B field. The gauge $\mathbf{A} = \mathbf{B} \times \mathbf{R}/2$ (parallel to $\mathbf{R}_y$) is chosen such that the wave vector $\mathbf{k} = -i\nabla + (e/ch)\mathbf{A}$. $\mathbf{R}$ is the vector from the center to the surface of the toroid. The TCN is very thin; hence, the vector potential at the toroid surface is approximated as a constant $\phi/2\pi R$. For an armchair (zigzag) TCN, wave vectors obtained from the transverse and the longitudinal periodical boundary conditions are $k_x = 2\pi J/3bm$ and $k_y = 2\pi(L + \phi/\phi_0)/\sqrt{3}bp$ [$k_x = 2\pi J/\sqrt{3}bm$ and $k_y = 2\pi(L + \phi/\phi_0)/3bp$]. $b = 1.42$ Å is the C-C bond length. $J = 1,2,\ldots,m$ and $L = 1,2,\ldots,p$ are the angular momenta, and they could serve as the state index. The electronic state energies of the armchair TCN are given by

$$E(J,L,\phi)_{\text{armchair}} = \pm\gamma_0\left\{1 \pm 4\cos\left(\frac{\pi J}{m}\right)\cos\left(\frac{\pi(L+\phi/\phi_0)}{p}\right) + 4\cos^2\left(\frac{\pi(L+\phi/\phi_0)}{p}\right)\right\}^{1/2}, \tag{1a}$$

and those of the zigzag TCN are given by

$$E(J,L,\phi)_{\text{zigzag}} = \pm\gamma_0\left\{1 \pm 4\cos\left(\frac{\pi J}{m}\right)\cos\left(\frac{\pi(L+\phi/\phi_0)}{p}\right) + 4\cos^2\left(\frac{\pi J}{m}\right)\right\}^{1/2}. \tag{1b}$$

The quantity $\gamma_0 = 3.033$ eV is the resonance integral for the nearest-neighbor interaction.[14] The states, with energies less (larger) than $E_F = 0$, are occupied (unoccupied) states, if the Zeeman splitting is absent. The $-(+)$ sign appearing outside the square-root sign corresponds to the occupied (unoccupied) states. On the other hand, the plus and minus signs inside the square-root sign are the unfolded and folded states, respectively.[14] That the $\pm$ signs are substituted by $+$ and $L = 1,2,\ldots,2p$ (or $J = 1,2,\ldots,2m$) is another equivalent choice. The J states, which are closest to the Fermi level $E_F = 0$, would dominate the low-frequency physical properties. For example, for an armchair TCN, the energy gap and the persistent current are principally determined by the $J = m$ states.

The electronic state energy should include the spin-B interaction, $E(\sigma,\phi) = g\sigma\phi/m^*R^2\phi_0$, i.e., $E(J,L,\sigma,\phi) = E(J,L,\phi) + E(\sigma,\phi)$. The g factor is taken to be the same as that ($\simeq 2$) of the pure graphite or GIC's.[20] $\sigma = \pm 1/2$ is the electron spin, and m^* is the bare electron mass. In general, the Zeeman spitting could be neglected except at very large

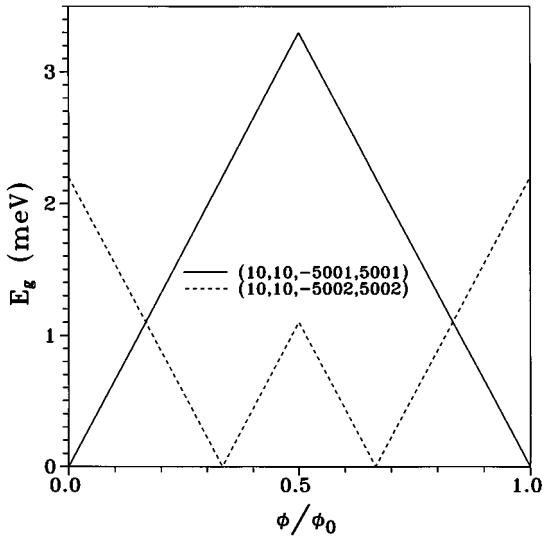

FIG. 2. The magnetic-flux-dependent energy gaps in the absence of the Zeeman splitting. The solid and dashed curves, respectively, are those of the (10,10,−5001,5001) (type I) and (10,10, −5002,5002) (type II) TCN's.

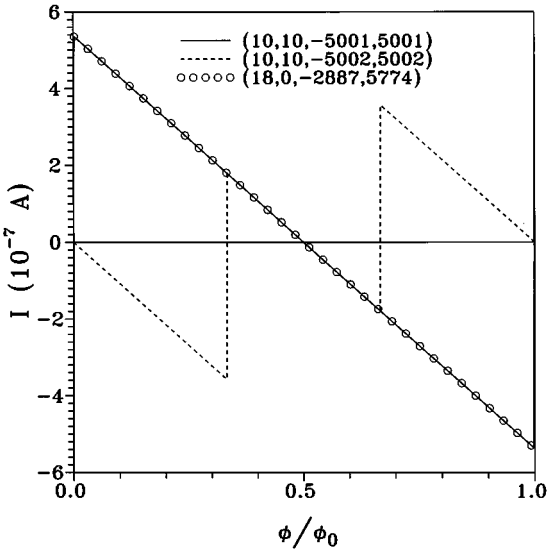

FIG. 3. The persistent currents in the absence of the Zeeman splitting are shown at $T=0$. The solid and dashed curves are those of the (10,10,−5001,5001) and (10,10,−5002,5002) TCN's separately. That of the (18,0,−2887,5774) TCN (the open circles) is also shown for the comparison.

ϕ, since it is inversely proportional to R^2. For example, $E(\sigma,\phi)\sim 2\,\mu$eV for the (10,10,−5001,5001) TCN at $\phi=\phi_0$.

The electronic structures at $\phi=0$ are first discussed. There are three types of electronic structures, which rely on the geometric structures. A type I TCN, which both m and p are the multiple of 3 ($3i$; i is an integer), is a metal.[15–16] The HOS and LUS meet with each other at $E_F=0$, e.g., the ($J=10$, $L=3334$) states of the (10,10,−5001,5001) TCN (the solid curve in Fig. 2). Moreover, density of states (DOS) is divergent in δ-function form there. For a type II TCN, m is equal to $3i$, but the opposite is true for p. It is a narrow-gap semiconductor with $E_g\sim 1$ meV, e.g., the (10,10, −5002,5002) TCN (the dashed curve in Fig. 2). A type III TCN defined by $m\neq 3i$ has a large energy gap, e.g., $E_g\sim 1.5$ eV for the (11,0,−5001,5001) TCN. Such a type of TCN is very insensitive to magnetic flux, so that the persistent currents are almost vanishing. Type I and II TCN's are the main object of study.

The low energy electronic structure of a (m,n,p,q) TCN could be understood from that of a (m,n) SCN. A TCN samples the π-electron states of a SCN, which satisfies the longitudinal boundary condition. When a SCN is metallic,[14–16] the edge state of the linear subbands is located at the Fermi level. If a TCN could (could not) sample such a state, it is a metal (a narrow-gap semiconductor). But when a SCN is semiconducting, a TCN must be a wide-gap semiconductor. Metallic or semiconducting TCN's are mainly determined the geometric structures.

The electronic states vary with magnetic flux. The ϕ-dependent states would exhibit the periodical oscillation, with a period ϕ_0, in the absence of the spin-B interaction. A type I TCN would change from a metal into a semiconductor as ϕ increases from zero, e.g., the (10,10,−5001,5001) TCN. The ϕ-dependent energy gap calculated from Eq. (1a) or (1b) is

$$E_g(\phi)=\begin{cases}\dfrac{3b\gamma_0}{R}\dfrac{\phi}{\phi_0} & \text{if } 0\leqslant\phi\leqslant\phi_0/2,\\[2ex] \dfrac{3b\gamma_0}{R}\dfrac{\phi_0-\phi}{\phi_0} & \text{if } \phi_0/2\leqslant\phi\leqslant\phi_0,\end{cases}\tag{2}$$

E_g is inversely proportional to the toroid radius; furthermore, it is symmetric about $\phi=\phi_0/2$. A type II TCN exhibits a similar oscillation, e.g., the (10,10,−5002,5002) TCN. Its energy gap is given by

$$E_g(\phi)=\begin{cases}\dfrac{3b\gamma_0}{R}\left|\dfrac{1}{3}-\dfrac{\phi}{\phi_0}\right| & \text{if } 0\leqslant\phi\leqslant\phi_0/2,\\[2ex] \dfrac{3b\gamma_0}{R}\left|\dfrac{2}{3}-\dfrac{\phi}{\phi_0}\right| & \text{if } \phi_0/2\leqslant\phi\leqslant\phi_0.\end{cases}\tag{3}$$

But on the other hand, there are two main differences between type I and II TCN's. One is that a type I TCN is a metal at $\phi_a=i\phi_0$, but a type II TCN at $\phi_a=(i\pm\frac{1}{3})\phi_0$. The metal-semiconductor transition happens at ϕ_a. The persistent current would exhibit a special jump structure there (Fig. 3). As a result of this difference, type I and type II TCN's might exhibit very different persistent currents, e.g., opposite magnetism at small ϕ. Another is that the maximum of E_g is, respectively, located at $\phi=\phi_0/2$ and $\phi=0$ for type I and II TCN's.

III. PERSISTENT CURRENTS

The electronic state energies in Eqs. (1a) and (1b) are used to study the characteristics of persistent currents. They vary with the magnetic flux through a TCN. The persistent current is the variation of free energy with the magnetic flux. The canonical ensemble (here, the same with the grand ca-

nonical ensemble) is taken in evaluating the free energy. The distribution probability of each electronic state is described by the Fermi-Dirac function

$$f[E(J,L,\sigma,\phi)]=\frac{1}{\exp\{\beta[E(J,L,\sigma,\phi)-\mu(T,\phi)]\}+1}, \tag{4}$$

where $\beta=(k_BT)^{-1}$. The chemical potential $\mu(T,\phi)$ is equal to zero at $T=0$. It remains so for any T and ϕ. The symmetric structure of occupied and unoccupied states could explain why $\mu(T,\phi)=0$. The chemical potential is independent of T and ϕ; therefore, a TCN only exchanges energy with a reservoir, i.e., the particle number is fixed during the variation of ϕ. The free energy at T is given by

$$F(\phi,T)=\sum_{\sigma,J,L}\frac{-1}{\beta}\ln\{1+\exp[-\beta E(J,L,\sigma,\phi)]\}. \tag{5}$$

The persistent current at T is calculated from the definition

$$I(\phi,T)=-c\frac{\partial F(\phi,T)}{\partial\phi}$$

$$=-c\sum_{\sigma,J,L}f[E(J,L,\sigma,\phi)]\frac{\partial E(J,L,\phi)}{\partial\phi}, \tag{6a}$$

where

$$\frac{\partial E(J,L,\phi)_{\text{armchair}}}{\partial\phi}=\frac{\mp 2\pi\gamma_0\sin[\pi(L+\phi/\phi_0)/p]\{\pm\cos(\pi J/m)+2\cos[\pi(L+\phi/\phi_0)/p]\}}{p\phi_0\sqrt{1\pm 4\cos(\pi J/m)\cos[\pi(L+\phi/\phi_0)/p]+4\cos^2[\pi(L+\phi/\phi_0)/p]}}, \tag{6b}$$

and

$$\frac{\partial E(J,L,\phi)_{\text{zigzag}}}{\partial\phi}=\frac{\mp 2\pi\gamma_0\sin[\pi(L+\phi/\phi_0)/p]\pm\cos(\pi J/m)]}{p\phi_0\sqrt{1\pm 4\cos(\pi J/m)\cos[\pi(L+\phi/\phi_0)/p]+4\cos^2(\pi J/m)}}. \tag{6c}$$

The persistent current in Eq. (6a) comes from the electronic orbital motion. The current $cg\sigma/m^*R^2\phi_0$ due to the spin magnetic moment is not included in Eq. (6a), since it is negligible. The effect of the Zeeman splitting, which is obvious only at large ϕ (Fig. 6), is reflected in the Fermi distribution. The spin-B interaction will be neglected in the following calculations except in a special case. The expression of $I(\phi,T)$ is complicated as seen from Eq. (6b) or (6c). The term $\partial E(J,L,\phi)/\partial\phi$ consists of both the angular momenta J and L. Consequently, the simply linear relation, as found in a mesoscopic ring,[4] between current carried by each state and angular momentum (L) is absent.

The ϕ-dependent persistent current at $T=0$ is first studied. It is caused by the electronic states with $E(J,L,\phi)\leqslant E_F$. The armchair TCN's are taken as the model systems to see the basic features. $I(\phi,T=0)$ in the (10,10,$-$5001,5001) (type I) TCN is shown in Fig. 3 by the solid curve. The persistent current is periodic with period ϕ_0, and it is antisymmetric about $\phi_0/2$. That is to say, $I(\phi,T=0)=I(\phi+\phi_0,T=0)=-I(\phi_0-\phi,T=0)$. Both periodicity and antisymmetry are easily identified from Eq. (6b).

The magnitude of I ($\sim 10^{-7}$ A) is small, i.e., the magnetic response of a TCN is weak. By the detailed analysis, the main contributions to the persistent current are found to come from the states ($J=m,L<p/3$) and ($J=m,L\geqslant 2p/3$) (details in the Appendix). Moreover, the currents carried by the two states L and $p-L$ would significantly cancel each other [the first terms in Eqs. (A4) and (A5)]. Such cancellations lead to the small net current, as seen in Fig. 3. The ϕ dependence of the persistent current, which is demonstrated to be linear [the second terms in Eqs. (A4) and (A5)], is described by

$$I(\phi)=I_0\left(\delta_{\phi=\phi_a}-\frac{2\phi}{\phi_0}\right)\quad\text{for } 0\leqslant\phi<\phi_0, \tag{7}$$

where $I_0=4\sqrt{3}\pi\gamma_0/p\phi_0$ is the amplitude of the AB oscillation, e.g., $I_0\sim 5.38\times 10^{-7}$ A for the (10,10,$-$5001,5001) TCN. There is a special jump structure at ϕ_a, where the metal-semiconductor transition occurs. Also notice that Eq. (7) keeps a similar form for the type II TCN. On the other hand, the contributions due to the states ($J=m,p/3\leqslant L<2p/3$) and ($J\neq m,L$) are almost vanishing. The currents, which are carried by the unfolded and folded states of ($J=m,p/3\leqslant L<2p/3$), have the same magnitude but the opposite direction. The net current due to them thus vanishes. Concerning the $J\neq m$ states, they are far from the Fermi level, so that their energies are insensitive to the variation of ϕ. Furthermore, the cancellations between the L and $p-L$ states remain significant at any ϕ. The net current carried by the $J\neq m$ states is negligible, which illustrates that the persistent current depends on the states relatively close to the Fermi level.[4]

The persistent current in the type II TCN exhibits similar characteristics; the periodicity, the antisymmetry, the weak response, the linear ϕ dependence, and the special jump structures, e.g., $I(\phi)$ of the (10,10,$-$5002,5002) TCN (the dashed curve in Fig. 3). However, there are two important differences between type I and II TCN's. First, the direction of current might be opposite. At small ϕ (>0), the current of the type I TCN is positive, while that of the type II TCN is negative. That is to say, the former and the latter is paramagnetic and diamagnetic, respectively. In general, the net current due to the ($J=m,L$) and ($J=m,p-L$) states is negative

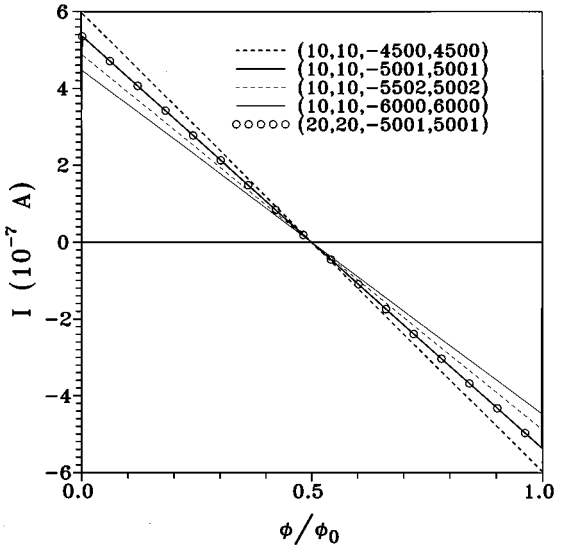

FIG. 4. Same plot as Fig. 3, but shown for TCN's with various radii. The persistent current of the (20,20,−5001,5001) TCN (the open circles) is also shown to see the dependence on the toroid width.

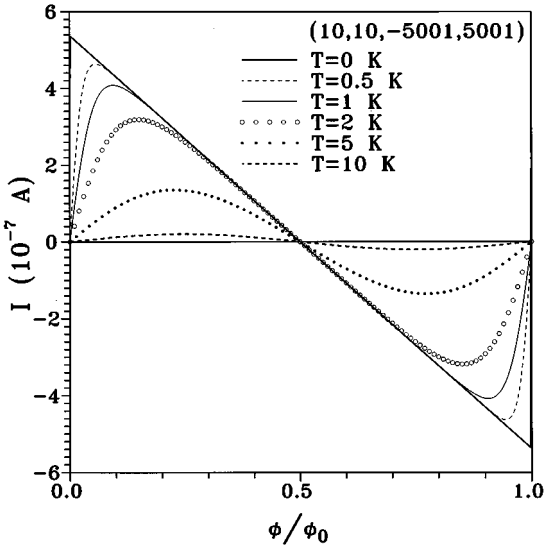

FIG. 5. Same plot as Fig. 3, but shown at various temperatures.

at any ϕ [the second terms in Eqs. (A4) and (A5)]. But for the ($J=m$, $L=2p/3$) state of the type I TCN, it could make a large and positive contribution (I_0) to the net current (Appendix). The main reason is that the current carried by the ($J=m$, $L=p/3$) state vanishes as ϕ increases from zero. Consequently, the paramagnetism of the type I TCN is purely caused by the ($J=m$, $L=2p/3$) state closest to the Fermi level. In addition, the opposite case would happen at $\phi<0$. Second, the special jump structures occur at different ϕ_a's, and the height of the jumps is different. They are, respectively, situated at $i\phi_0$ and $(i\pm\frac{1}{3})\phi_0$ for type I and II TCN's [Eq. (7)]. These jumps are related to the metal-semiconductor transitions or vice versa. Their cause is similar to that of the paramagnetism of the type I TCN. When ϕ increases from the left-hand neighborhood to the right-hand neighborhood of ϕ_a, the two states, $L_a=p/3-\phi_a/\phi_0$ and $L_b=2p/3-\phi_a/\phi_0$, would induce a jump of $2I_0$ (I_0) in the type I TCN (the type II TCN separately). For example, for the (10,10,−5002,5002) TCN, the jumps of I_0 at $\phi_0/3$ and $2\phi_0/3$ result from the $L=1667$ and $L=3334$ states, respectively.

The above-mentioned characteristics of the persistent currents are obtained for the armchair TCN's. Similar results could also be found in the zigzag TCN's. For example, the zigzag TCN defined by (18,0,−2887,5774) (the open circles in Fig. 3) and the armchair TCN defined by (10,10, −5001,5001) have the same persistent current. That they both belong to the type I TCN, and they have the same radius (see below) could explain this result. In short, the geometric structure affects the electronic structure and thus the persistent currents.

We further see the effects due to the geometric structure (such as radius and width), the temperature, and the Zeeman splitting. The persistent currents are shown in Fig. 4 for various TCN's. They are inversely proportional to the toroid radius, but independent of the toroid width. These results could be understood from Eq. (7), in which $I(\phi)$ depends on p^{-1}, but not m^{-1}. The induced magnetic moment $\pi R^2 I(\phi)$ is further identified to be proportional to the toroid radius. The larger the TCN is, the stronger the magnetic response. A larger TCN is suggested to be more suitable in the experimental verification of the AB effect. The magnitude of the magnetic moment is $\sim 5\times 10^{-20}$ A m^2 for a TCN with $R\sim 2000$ Å. It is much larger than that ($<10^{-20}$ A m^2) in a mesoscopic ring.[4–7] Hence the characteristics of the persistent currents in TCN's could be verified from the magnetic measurements.

When temperature increases from zero, electrons would occupy the states above the Fermi level [$E(J,L,\phi)>0$]. Such states produce the persistent current, which the direction of current is opposite to that of the states below the Fermi level [Eq. (6b)]. The cancellations between the states below and above the Fermi level obviously increase with T. Therefore, the oscillational amplitude of the ϕ-dependent persistent current declines rapidly in the increasing of T (Fig. 5). The jump structures would be replaced by the peak structures owing to the thermal broadening. But on the other hand, temperature does not destroy the periodicity of the AB oscillation, since it does not affect the electronic structure in Eq. (1a). The persistent current would become too small to be observable at higher temperatures, e.g., $T\geqslant 10$ K. The low-temperature magnetic measurements are needed for the verification of the AB effect in TCN's.

The spin-B interaction $E(\sigma,\phi)$ needs to be taken into account at large ϕ, e.g., $\phi\sim 100\phi_0$ (or $B\sim 3$ T). The persistent currents including the Zeeman splitting are shown in Fig. 6 at $100\phi_0\leqslant\phi\leqslant 102\phi_0$ and $T=0$. Compared with that in Fig. 3, the periodical oscillation is apparently destroyed by the inclusion of the spin-B interaction. As a result of $E(\sigma,\phi)$, the energy of the spin-down state becomes lower, while that of the spin-up state becomes higher. The Zeeman splitting could make certain states cross the Fermi level at magnetic flux smaller ($\phi_{c,-}$) and larger ($\phi_{c,+}$) than ϕ_a. The metal-semiconductor or semiconductor-metal transitions would occur more frequently, which thus induces more jump structures in the persistent current and destruction of the periodicity.

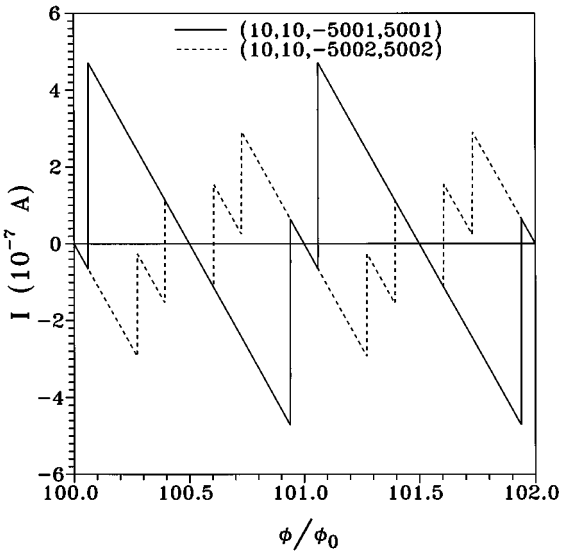

FIG. 6. Same plot as Fig. 3, but the Zeeman splitting is taken into account.

A single jump at ϕ_a is replaced by a pair of jumps at $\phi_{c,\mp}$, which is related to the state crossing of the Fermi level. The crossing positions $\phi_{c,\mp}$ satisfy the condition $E(m,L,\phi_{c,\mp})=E(\sigma,\phi_{c,\mp})$. An approximate $\phi_{c,\mp}$ could be obtained from expanding $E(m,L,\phi)$ in the neighborhood of ϕ_a, where L is equal to $L_a=p/3-\phi_a/\phi_0$ or $L_b=2p/3-\phi_a/\phi_0$. $\phi_{c,\mp}$ is approximately given by

$$\phi_{c,\mp}\approx\left(1\mp\frac{2g\sigma}{3bR\gamma_0 m^*}\right)\phi_a. \tag{8}$$

The magnetic-flux region, in which a pair of jumps exist, is $\sim 0.12\phi_0$ for $\phi_a=101\phi_0$. The persistent current exhibits the special jumps at $\phi_{c,\mp}$, since certain states become occupied or unoccupied in the increasing of ϕ. Here we examine the jumps at $\phi_{c,-}$, and the similar result is obtained for the jumps at $\phi_{c,+}$. The unfolded (folded) spin-up state for $E(m,L_a,\phi)<0[E(m,L_b,\phi)<0]$ changes into an unoccupied state, but the unfolded (folded) spin-down state for $E(m,L_a,\phi)>0[E(m,L_b,\phi)>0]$ changes into an occupied state. The former and the latter, respectively, carry current $-I_0/4$ and $I_0/4$ [Eqs. (A4) and (A5)], so they cause a jump of $I_0/2$ at the crossing position. For the type I (type II TCN's, the L_a and L_b states would contribute to the jump of current at the same (different) position, as stated earlier. Hence the height of jumps, as seen in Fig. 6, is I_0 and $I_0/2$ for type I and II TCN's separately. On the contrary, the persistent current is independent of the Zeeman splitting, if the magnetic flux is located outside the region confined by $\phi_{c,-}$ and $\phi_{c,+}$. In summary, the persistent current linearly decreases with magnetic flux, together with the special jumps. At large ϕ, it could be expressed by

$$I(\phi)=I_0\left\{C\,\delta_{\phi=\phi_{c,\mp}}-\frac{2(\phi-i\phi_0)}{\phi_0}\right\}$$

$$\text{for } i\phi_0\leqslant\phi<(i+1)\phi_0, \tag{9}$$

where C is 1 and $\frac{1}{2}$ for type I and II TCN's respectively.

Finally, the magnetic response in TCN's is compared with that in SCN's. They exhibit the similar magnetism at small ϕ. Carbon nanotubes, which are metals at $\phi=0$, are paramagnetic, and the others are diamagnetic. On the other hand, the dependence on the nanotube radius, the temperature, and the Zeeman splitting might be different. The induced magnetic moment in TCN's is proportional to radius, while that in SCN's is insensitive to radius.[8–10] The former is expected to be observable at $T<10$ K. Such a temperature is much lower than that ($T<100$ K) for the latter.[10] The Zeeman effect only causes the more jump structures in TCN's; however, it causes the special cusps in SCN's. That DOS of TCN's and SCN's, respectively, diverges in δ-function and $1/\sqrt{E}$ forms leads to the difference in special structures.[10]

IV. CONCLUDING REMARKS

In this work, we have studied the electronic structure of the TCN's, and investigated the persistent currents in them. The comparison with SCN's and mesoscopic rings is also made.

The geometric structure determines the electronic structure and thus the characteristics of the persistent currents. The electronic structure calculated from the tight-binding model could be divided into three kinds of type according to the geometric structure. At $\phi=0$, the type I, II, and III TCN's are a metal, a narrow-gap semiconductor with $E_g\sim 1$ meV, and a wide-gap semiconductor with $E_g\sim 1$ eV, respectively. When TCN's are threaded by a uniform perpendicular B field, the persistent currents only exist in the type I and II TCN's. Such TCN's would drastically change from metals (semiconductors) into semiconductors (metals) during the variation of ϕ.

The main features of the ϕ-dependent persistent current include the periodical oscillation with a period ϕ_0, the antisymmetric structure about $(i-1/2)\phi_0$, the linear ϕ-dependence, the special jump structures, and the weak magnetic response. The periodical persistent current is the manifestation of the Aharonov-Bohm (AB) effect. Type I TCN's exhibit the paramagnetism at small ϕ, which contrasts greatly with the diamagnetism of type II TCN's. The magnetic moment due to the persistent current is small, while it is much larger than that of a mesoscopic semiconductor or metal ring. The magnetic measurements[5–7] could be used to verify the above mentioned characteristics.

The dependence of the persistent current on the toroid radius, the temperature, and the Zeeman splitting might be strong. The induced magnetic moment is found to be proportional to the toroid radius, but not the toroid width. On the other hand, the magnetic response of a SCN hardly depends on the radius.[8–10] The persistent current could exist at $T<5$ K. It would quickly decrease with an increase of T, however, temperature does not destroy the periodical AB oscillation. The Zeeman effect, which may lead to the destruction of the periodicity and more jump structures, is obvious only at very large ϕ. In short, a larger TCN at lower T and ϕ is relatively suitable in verifying the AB effect.

If TCN's are further connected by leads, they might display the quantized ballistic transport properties.[21] The electronic structure will be directly reflected in the transport behavior. The further theoretical and experimental studies on transport properties are very important.

ACKNOWLEDGMENTS

One of us (M.F.L.) thanks C. Cheng for helpful discussions. This work was supported in part by the National Science Council of Taiwan, Republic of China under Grant Nos. NSC 87-2112-M-006-019 and NSC 87-2112-M-009-009.

APPENDIX

The ϕ-dependent persistent current at $T=0$ is calculated here. The persistent current in the armchair TCN is given by

$$I(\phi)_{\text{armchair}} = -c \sum_{\sigma, J=m, L} \frac{2\pi\gamma_0 \sin[\pi(L+\phi/\phi_0)/p]\{\mp 1 + 2\cos[\pi(L+\phi/\phi_0)/p]\}}{p\phi_0 |1 \mp 2\cos[\pi(L+\phi/\phi_0)/p]|}. \tag{A1}$$

The current is due to the electronic states of $E(J=m,L,\phi) \leqslant 0$. The small-$\phi$ expansion is used to evaluate $I(\phi)$ at $0 \leqslant \phi < \phi_0$, i.e.,

$$\sin\left(\frac{\pi(L+\phi/\phi_0)}{p}\right) \simeq \sin\left(\frac{\pi L}{p}\right) + \frac{\pi\phi}{p\phi_0}\cos\left(\frac{\pi L}{p}\right), \tag{A2}$$

$$\cos\left(\frac{\pi(L+\phi/\phi_0)}{p}\right) \simeq \cos\left(\frac{\pi L}{p}\right) + \frac{\pi\phi}{p\phi_0}\sin\left(\frac{\pi L}{p}\right). \tag{A3}$$

This approximate expansion is reasonable because of $\pi\phi/p\phi_0 \ll 1$.

According to the denominator in Eq. (A1), the various L states are divided into $1 \leqslant L+\phi/\phi_0 < p/3$, $2p/3 \leqslant L+\phi/\phi_0$, and $p/3 \leqslant L+\phi/\phi_0 < 2p/3$. For the $1 \leqslant L+\phi/\phi_0 < p/3$ states, the current of the unfolded state [$-$ in Eq. (A1)] is the same with that of the folded state [$+$ in Eq. (A1)], and is given by

$$\frac{-I_0}{\sqrt{3}}\left\{\sin\left(\frac{\pi L}{p}\right) + \frac{\pi\phi}{p\phi_0}\cos\left(\frac{\pi L}{p}\right)\right\}. \tag{A4}$$

The two spin states have been included in Eq. (A4). Similar results are obtained for the $2p/3 \leqslant L+\phi/\phi_0$ states. The current carried by the unfolded or folded state is

$$\frac{I_0}{\sqrt{3}}\left\{\sin\left(\frac{\pi L}{p}\right) + \frac{\pi\phi}{p\phi_0}\cos\left(\frac{\pi L}{p}\right)\right\}. \tag{A5}$$

But for the $p/3 < L+\phi/\phi_0 < 2p/3$ states, the unfolded and the folded states carry currents similar to Eqs. (A5) and (A4), respectively. The net current from these two states thus vanishes.

The first terms in Eqs. (A4) and (A5) would cancel each other for the two states L and $p-L$ except for the states $L_a+\phi_a/\phi_0 = p/3$ and (or) $L_b+\phi_a/\phi_0 = 2p/3$. The significant cancellation is the principal cause of the weak magnetic response. On the other hand, the L_a and (or) L_b states, as seen in Fig. 3, would induce a special jump of $2I_0$ (I_0) at ϕ_a for type I (type II) TCN's. Concerning the second terms in Eqs. (A4) and (A5), the net current due to them is $-2I_0\phi/\phi_0$ after the summation of L's. Hence the ϕ-dependent persistent current declines at a rate $-2I_0/\phi_0$ except at ϕ's, where the metal-semiconductor transitions occur. This feature remains unchanged even in the presence of the Zeeman splitting. In short, $I(\phi)$ [Eq. (7)] is a linear dispersion relation, together with special jumps. While the Zeeman splitting is taken into account, the persistent current in the magnetic-flux region confined by $\phi_{c,\mp}$ would change. The results in Eqs. (A4) and (A5) could also be applied to understand the main change.

[1] S. Iijima, Nature (London) **354**, 56 (1991).
[2] A. Thess *et al.*, Science **273**, 438 (1996).
[3] J. Liu, H. Dai, J. H. Hafner, D. T. Colbert, R. E. Samlley, S. J. Tans, and C. Dekker, Nature (London) **385**, 780 (1997).
[4] H. F. Cheung, Y. Gefen, E. K. Riedel, and W. H. Shih, Phys. Rev. B **37**, 6050 (1988).
[5] L. P. Levy, G. Dolan, J. Dunsmuir, and H. Bouchiat, Phys. Rev. Lett. **64**, 2074 (1990).
[6] V. Chandrasekhar, R. A. Webb, M. J. Brady, M. B. Ketchen, W. J. Gallagher, and A. Kleinsasser, Phys. Rev. Lett. **64**, 3578 (1991).
[7] D. Mailly, C. Chapelier, and A. Benoit, Phys. Rev. Lett. **70**, 2020 (1993).
[8] H. Ajiki and T. Ando, J. Phys. Soc. Jpn. **62**, 2470 (1993); **64**, 4382 (1995).
[9] J. P. Lu, Phys. Rev. Lett. **71**, 1123 (1995).
[10] M. F. Lin and K. W.-K. Shung, Phys. Rev. B **52**, 8423 (1995).
[11] B. I. Dunlap, Phys. Rev. B **46**, 1933 (1992).
[12] S. Itoh, S. Ihara, and J. I. Kitakami, Phys. Rev. B **47**, 1703 (1993); **47**, 12 908 (1993).
[13] P. R. Wallace, Phys. Rev. **71**, 622 (1947).
[14] R. Saito, M. Fujita, G. Dresselhaus, and M. S. Dresselhaus, Appl. Phys. Lett. **60**, 2204 (1992); Phys. Rev. B **46**, 1804 (1992).
[15] J. W. Mintwire, B. I. Dunlap, and C. T. White, Phys. Rev. Lett. **68**, 631 (1992).
[16] N. Hamada, S. I. Sawada, and A. Oshiyama, Phys. Rev. Lett. **68**, 1579 (1992).
[17] R. C. Haddon, Nature (London) **388**, 31 (1997).
[18] D. H. Robertson, D. W. Brenner, and J. W. K. Mintmire, Phys. Rev. B **45**, 12 592 (1992).
[19] B. I. Dunlap, Phys. Rev. B **49**, 5643 (1994).
[20] M. S. Dresselhaus and G. Dresselhaus, Adv. Phys. **30**, 139 (1981).
[21] R. Landauer, IBM J. Res. Dev. **1**, 223 (1957); Philos. Mag. **21**, 863 (1970).